PNAS RESEARCH ARTICLE | NEUROSCIENCE OPEN ACCESS

Early death in a mouse model of Alzheimer's disease exacerbated by microglial loss of TAM receptor signaling

Youtong Huang[a,1] and Greg Lemke[a,2]

Edited by Marco Colonna, Washington University in St. Louis School of Medicine, St. Louis, MO; received March 10, 2022; accepted July 23, 2022

Recurrent seizure is a common comorbidity in early-stage Alzheimer's disease (AD) and may contribute to AD pathogenesis and cognitive decline. Similarly, many mouse models of Alzheimer's disease that overproduce amyloid beta are prone to epileptiform seizures that may result in early sudden death. We studied one such model, designated *APP/PS1*, and found that mutation of the TAM receptor tyrosine kinase (RTK) Mer or its ligand Gas6 greatly exacerbated early death. Lethality was tied to violent seizures that appeared to initiate in the dentate gyrus (DG) of the hippocampus, where Mer plays an essential role in the microglial phagocytosis of both apoptotic and newborn cells normally generated during adult neurogenesis. We found that newborn DG neurons and excitatory synapses between the DG and the cornu ammonis field 3 (CA3) field of the hippocampus were increased in TAM-deficient mice, and that premature death and adult neurogenesis in these mice were coincident. In contrast, the incidence of lethal seizures and the deposition of dense-core amyloid plaques were strongly anticorrelated. Together, these results argue that TAM-mediated phagocytosis sculpts synaptic connectivity in the hippocampus, and that seizure-inducing amyloid beta polymers are present prior to the formation of dense-core plaques.

microglia | hippocampus | adult neurogenesis | seizures | *Mertk*

Significance

Most patients with Alzheimer's disease (AD), a neurodegenerative disorder that leads to severe cognitive decline, suffer from concomitant seizures. These events also occur in mouse models of AD in which amyloid beta peptides are overproduced and are often lethal. Here we report the surprising finding that mutations in the TAM receptor tyrosine kinase system greatly exacerbate the incidence of lethal seizures in the *APP/PS1* mouse AD model. This exacerbation is tied to TAM activity in microglia during adult neurogenesis in the hippocampus, a trigger site for seizures generally, and results in the development of exuberant excitatory synapses in this critical brain region.

Alzheimer's disease (AD), the most prevalent neurogenerative disease and most common cause of human dementia, is associated with seizures. Unprovoked seizures are substantially more frequent in sporadic AD patients compared to age-matched nondemented populations (1–6) and are exceptionally prominent in early stages of early-onset familial AD (4, 7, 8). In addition, subclinical epileptiform activity has been detected by long-term electroencephalography (EEG) in more than 40% of AD patients, where it is correlated with accelerated cognitive decline (9). This abnormal network activity often begins decades before the symptomatic onset of AD (10, 11). Correspondingly, many amyloidogenic mouse models of AD that rely on the elevated production of amyloid beta (Aβ) peptides—as a result of transgenic expression of mutant forms of the human amyloid precursor protein (APP) and/or the presenilin 1 (PSEN1) component of the APP gamma secretase—also display cortical and hippocampal hyperexcitability and experience unprovoked seizures early in disease before the appearance of Aβ plaques (12–19).

We have recently published analyses of one such mouse—the *APP/PS1* line that carries an amyloidogenic "Swedish" mutation in the human *APP* gene and a pathogenic mutation in the human *PSEN1* gene (20–22). Although not routinely addressed in the literature, it is well documented that *APP/PS1* populations on a C57BL/6 background exhibit 10 to 15% mortality due to sudden death early in life (12, 13). This sudden death, which is not associated with any gross postmortem neuropathology, has been found to be the result of lethal epileptic seizures (12). These seizures are in turn linked to markedly higher levels of interictal spiking of cortical pyramidal neurons, as detected by EEG, patch clamp recording in cortical slices, and implanted electrodes in vivo (12).

In our previous studies (22), we examined the effects of germline loss-of-function mutations in the mouse genes encoding the TAM receptor tyrosine kinases (RTKs) Mer and Axl (23, 24), and their ligand Gas6 (25), when crossed into *APP/PS1*. In the current analysis, we found that mutation of Mer (gene name *Mertk*), Gas6, or Axl and Mer together all led to a marked exacerbation of early sudden death in both sexes. Importantly, this was also seen for *APP/PS1* compound mutants that carried microglial-restricted mutations in *Mertk*. As for *APP/PS1* alone, nearly all sudden death in the compound mutants occurred before postnatal day (P)150, after which time all populations were stable. Video recording in our colonies demonstrated that the compound mutants died from the same spontaneous epileptic seizures that have been shown to kill young *APP/PS1* mice. Analyses of the activation marker Arc immediately following lethal seizures were consistent with these seizures being initiated in the dentate gyrus (DG) of the hippocampus.

Author affiliations: [a]Molecular Neurobiology Laboratory, Salk Institute for Biological Studies, La Jolla, CA 92037

Author contributions: Y.H. and G.L. designed research; Y.H. performed research; Y.H. contributed new reagents/analytic tools; Y.H. and G.L. analyzed data; and G.L. wrote the paper.

The authors declare no competing interest.

This article is a PNAS Direct Submission.

[1]Present address: F.M. Kirby Center for Neurobiology, Boston Children's Hospital, Boston, MA 02115.

[2]To whom correspondence may be addressed. Email: lemke@salk.edu.

This article contains supporting information online at http://www.pnas.org/lookup/suppl/doi:10.1073/pnas.2204306119/-/DCSupplemental.

Published October 3, 2022.

Together with the subventricular zone (SVZ) adjacent to the lateral ventricle, the DG harbors a prominent site of adult neurogenesis in the mouse (26, 27). At both sites, microglial Mer has been shown to play an essential role in the phagocytic clearance of the large number of apoptotic cells (ACs) that are generated during this process (28, 29). Importantly, the bulk of adult neurogenesis and AC generation in the mouse occurs over a delimited developmental window between birth and P150 (26), the same window in which *APP/PS1* mice die from seizures. During this time, Mer-expressing microglia also phagocytose live newborn cells that express the "eat-me" signal phosphatidylserine (PtdSer) (29, 30). In the SVZ, TAM mutations have been shown to result in the survival of many of these newborn cells, which would otherwise have been "eaten alive," and in their integration as viable differentiated neurons in the olfactory bulb (29). Consistent with these earlier findings, we observed that *APP/PS1* mice lacking both Axl and Mer displayed 6-fold more ACs and 2.1-fold more viable 5-bromo-2-deoxyuridine (BrdU)-labeled cells in the DG at 4 wk after a BrdU pulse than did *APP/PS1* mice alone. Moreover, these TAM-deficient *APP/PS1* mice also displayed a 1.4-fold increase, relative to their *APP/PS1* counterparts, in excitatory connections between DG granule cell neurons and their synaptic targets in the cornu ammonis field 3 (CA3) of the hippocampus. Taken together, these results indicate that the loss of TAM signaling exacerbates the preexisting hyperexcitability of *APP/PS1* mice via increased excitatory connections between the DG and CA3, and that TAM-mediated microglial phagocytosis is normally required for the proper sculpting of these hippocampal circuits during adult neurogenesis.

Results

Early Lethality in *APP/PS1* Is Exacerbated by *Mertk* and *Gas6* Mutation. We monitored and plotted the survival of *APP/PS1* mice on C57BL/6J over the first 200 d of postnatal life and quantified the loss of ∼15% of the *APP/PS1* colony by P150 (Fig. 1). This is in close agreement with previous reports of early sudden death in this line, which has been linked unequivocally to lethal tonic–clonic seizures (12, 13). For example, recordings from electrodes implanted into both *APP/PS1* cortices have consistently detected profound and chronic epileptiform activity, with 65% of *APP/PS*1 mice experiencing at least one large electrographic seizure by 19 wk of age (12). Similarly, 24-h video monitoring has revealed that 83% of compound *APP/PS1* mutants experiencing a grand mal seizure die immediately from the observed seizure (13). Treatment with the anticonvulsant levetiracetam, which suppresses seizures, entirely suppresses early sudden death in these mice; and conversely, treatment with the noncompetitive $GABA_A$ inhibitor picrotoxin, which antagonizes inhibitory neuronal signaling, increases seizure activity and exacerbates early sudden death (13). In contrast to *APP/PS1* mice, mutants lacking both Mer and Axl ($Axl^{-/-}Mertk^{-/-}$), the TAM receptors expressed by microglia (22, 29), together with mice lacking the universal TAM ligand Gas6 ($Gas6^{-/-}$) (25, 31), all displayed normal wild-type (WT) (100%) viability well beyond P200 (Fig. 1), also as reported previously (23, 24, 32).

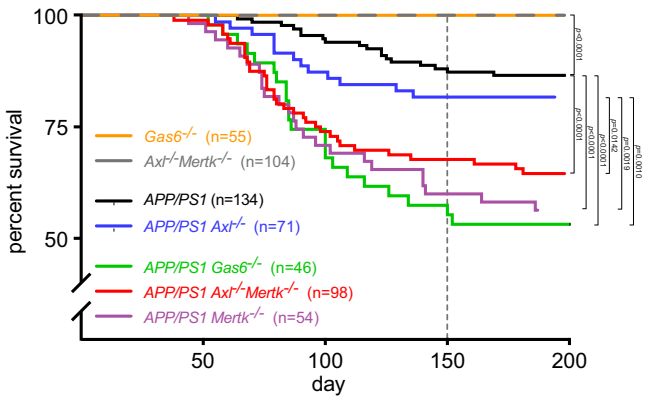

Fig. 1. TAM mutations exacerbate early lethality in *APP/PS1* mice. Percent survival of mouse populations of the indicated genotypes and indicated sizes (*n* = number of mice monitored) as a function of age (postnatal day). Dotted vertical indicates the time at which Aβ plaques are reliably detected in the *APP/PS1* line. Indicated *P* values calculated by log-rank test. In this and all subsequent figures, differences that are not statistically significant do not have a specified *P* value.

Although TAM system mutations on their own were without effect on viability, crossing these mutations into the *APP/PS1* line greatly exacerbated its early sudden death. Introducing the $Axl^{-/-}$ single mutation yielded a trend toward increased lethality, but this effect was not statistically different from the course of death seen in *APP/PS1* alone when evaluated using the log-rank test (Fig. 1; $P = 0.3012$). In marked contrast, introduction of $Mertk^{-/-}$ or $Axl^{-/-}Mertk^{-/-}$ or $Gas6^{-/-}$ mutations into *APP/PS1* all resulted in the death of ≥40% of the compound mutants by P150, and this exacerbation of early lethality relative to *APP/PS1* was highly significant (Fig. 1). Sudden death in $APP/PS1Mertk^{-/-}$, $APP/PS1Axl^{-/-}Mertk^{-/-}$, and $APP/PS1Gas6^{-/-}$ mice was first observed at or just before P50 and progressed at the same consistent rate in all three genotypes until ∼P120 (Fig. 1). After ∼P150 (dotted vertical line in Fig. 1), sudden death in all populations largely ceased. This has also been previously documented for *APP/PS1* alone, whose populations are subsequently stable (100% viable) through at least 10 mo (13).

The two most prominent cellular loci for Mer expression in the adult brain are microglia, the specialized tissue macrophages of the central nervous system, and endothelial cells of the blood vasculature (22, 29, 33). To assess the relative importance of these two cell types to the $APP/PS1Mertk^{-/-}$ lethality reported in Fig. 1, we crossed conditional floxed alleles of the *Mertk* gene (29) into a tamoxifen-inducible $Cx3cr1^{CreER}$ driver line (34) and then crossed these mice with *APP/PS1*. The $Cx3cr1^{CreER/+}Mertk^{f/f}$ mutants allow for tamoxifen-induced microglial *Mertk* inactivation and endothelial cell preservation of *Mertk* expression in the brain (29). When we injected corn oil control into $APP/PS1Cx3cr1^{CreER/+}Mertk^{f/f}$ mice immediately after weaning (at P30 to 40), we observed an onset and progression of sudden death that closely paralleled that seen in *APP/PS1* (*SI Appendix*, Fig. S1). In contrast, when we injected tamoxifen into these same mice, we observed a sudden death time course that paralleled that seen in $APP/PS1Mertk^{-/-}$ mice (*SI Appendix*, Fig. S1). Although brain (and other) perivascular macrophages are also $Cx3cr1^{+}$ and weakly express Mer (35), these cells account for <3% of the $CD45^{+}$ cells in the adult brain and are vastly outnumbered by $Mer^{+}Cx3cr1^{+}$ microglia (36). We therefore conclude that the cells that drive the sudden death in the germline $APP/PS1Mertk^{-/-}$ mutants are microglia. These brain macrophages respond to and regulate neuronal activity (37, 38) and are strongly activated, especially in the hippocampus, subsequent to seizures (39–41). As discussed below, they are also exceptionally active TAM-dependent phagocytes (29).

The major contribution of Mer mutation and the minor contribution of Axl mutation to enhanced early lethality in the

APP/PS1 compound mutants (Fig. 1) are both consistent with the fact that microglia normally express high levels of Mer and low levels of Axl (22, 29). (In contrast, perivascular macrophages express high levels of Axl and low levels of Mer) (35). Although microglial Axl is markedly up-regulated in *APP/PS1* and other mouse AD lines (22, 36) and in human AD (42), this up-regulation occurs exclusively in microglia that are tightly bound to Aβ plaques (22, 43). The first deposition of Aβ plaques in the cortex and hippocampus of *APP/PS1* mice is observed at ∼P120, and plaques are not reliably detected across the brain in these mice until ∼P150 (44, 45). Thus, nearly all of the sudden death quantified in Fig. 1 occurred before the initial deposition of Aβ plaques and the up-regulation of Axl. Indeed, as detailed below, sudden death and the development of plaques were strongly anticorrelated in all genotypes. Although the contribution of *Axl* mutation to enhanced *APP/PS1* lethality was minimal, most comparative analyses below were performed with $Axl^{-/-}Mertk^{-/-}$ compound mutants to ensure complete TAM inactivation.

***APP/PS1Mertk*$^{-/-}$ Seizures Are Associated with Massive Firing of the Dentate Gyrus.** As noted above, prior analyses demonstrated that young *APP/PS1* mice display repeated episodes of cortical epileptiform seizure activity and experience tonic–clonic seizures that very frequently lead to acute sudden death (12, 13). These events result from the overproduction of Aβ (19), which triggers cortical and hippocampal hyperexcitability via sustained elevation of the resting membrane potential of layer 2/3 pyramidal neurons and dentate granule cells, respectively (12). As also noted above, seizures are a recognized comorbidity at early stages of human AD (46, 47). Continuous video monitoring of $APP/PS1Axl^{-/-}Mertk^{-/-}$ and $APP/PS1Mertk^{-/-}$ mice indicated that sudden death in these compound mutants was, consistent with the previous reports discussed above, also the result of violent tonic–clonic seizures (*SI Appendix*, Movies S1 and S2 and Fig. S2*A*).

The V-shaped DG of the hippocampus normally displays low spiking activity and is thought to function as an inhibitory gate that limits excitatory input to the remainder of the hippocampus. It is a common initiating locus for temporal lobe epilepsy in humans and mice (48–50), when this gating is weakened and granule cells become hyperexcitable. We did not perform any manipulation to induce seizures in our colonies and so routinely encountered $APP/PS1Mertk^{-/-}$, $APP/PS1Axl^{-/-}Mertk^{-/-}$, and $APP/PS1Gas6^{-/-}$ mice that had died overnight. Although brains from these long-dead animals could not be analyzed (decomposition begins within minutes of death), we fortuitously encountered four $APP/PS1Mertk^{-/-}$ mice during or immediately after a spontaneous lethal seizure. Immunostaining for the transcription factor Arc (Arg3.1), an established marker of neuronal activity (51), demonstrated massive firing of all of the granule cells in the DG in these mice (Fig. 2 *A*, *Top*). (In contrast to our normal immunohistochemical analyses, which were performed on sections cut from perfusion-fixed brains, this Arc immunostaining was performed on sections cut from immersion-fixed brains removed shortly after death. All representative panels from both of the genotypes in Fig. 2 and *SI Appendix*, Fig. S2 are from sections of immersion-fixed material.) In addition to the DG, widespread high Arc staining was evident in $NeuN^+$ neurons across many loci of the $APP/PS1Mertk^{-/-}$ brain after seizure, including the CA3 field of the hippocampus, cortex, striatum, hypothalamus, superior colliculus, and olfactory bulb (Fig. 2 *A*, *Top* and *SI Appendix*, Fig. S2*B*).

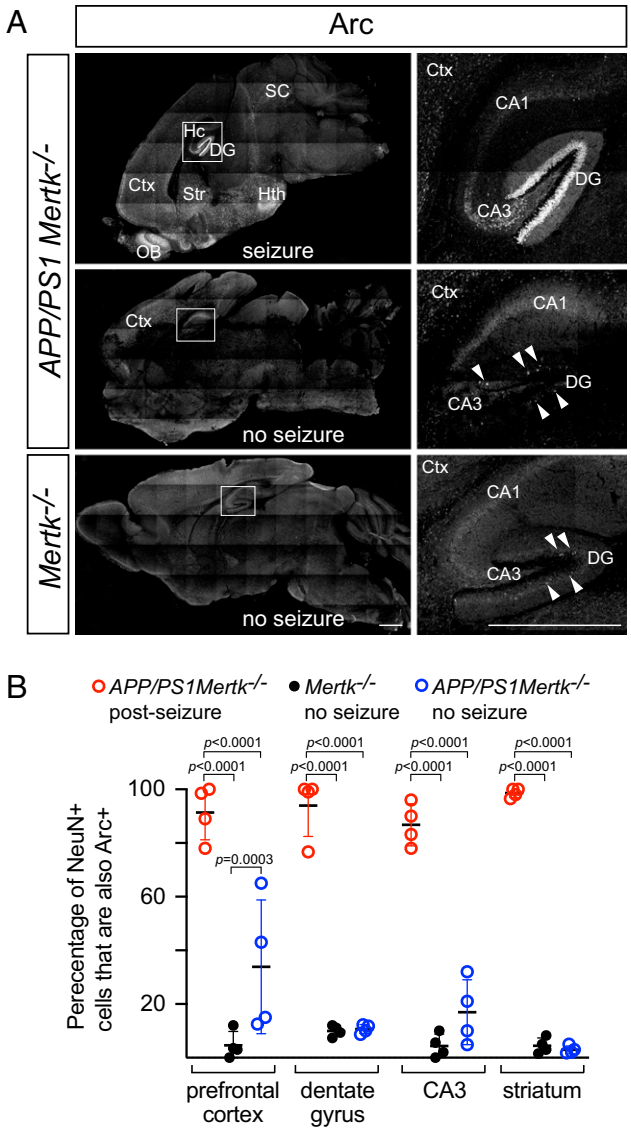

Fig. 2. Massive neuronal firing in the $APP/PS1Mertk^{-/-}$ dentate gyrus after seizure. (*A*) Sagittal sections of the brains of mice of the indicated genotypes either immediately after lethal seizure (seizure) or in the absence of seizure (no seizure). Recent neuronal firing is assessed by immunostaining of sections with an antibody to the transcription factor Arc (white signal), whose expression is transiently induced following neuronal depolarization. Panels on the *Right* are enlargements of boxed regions in the *Left* panels. Abbreviations: DG, dentate gyrus; Hc, hippocampus; SC, superior colliculus; Hth, hypothalamus; Ctx, cortex; Str, striatum; OB, olfactory bulb. CA1 and CA3 are fields of the hippocampus. CA3, which receives direct connections from the DG, is also strongly activated after seizure. Representative images from four mice. (Scale bars, 1 mm.) (*B*) Quantification of the fraction of $NeuN^+$ neurons that were Arc^+ in the indicated regions of mice of the indicated genotypes, with or without seizure. Each data point is the average of two images per region per mouse (two sections per mouse and four mice per genotype and condition). Two-way analysis of variance (ANOVA) test.

This widespread Arc expression stood in marked contrast to that seen in mice of the same genotype in the absence of seizure (Fig. 2 *A*, *Middle*). In these animals, Arc^+ loci of neuronal firing were still evident in the cortex (*SI Appendix*, Fig. S2*C*), suggestive of a basal level of network hyperactivation, but the massive activation of all neurons in the DG was not seen. Instead, only occasional DG cells were Arc^+ (Fig. 2 *A*, *Middle Right*), consistent with the normally sparse Arc expression and firing of DG granule cells that has been documented for wild-type mice (50, 52, 53). This same sparse expression of Arc in the DG was also seen in $Mertk^{-/-}$ mice (Fig. 2 *A*, *Bottom*).

Importantly with respect to the results presented below, these *Mertk*$^{-/-}$ mice displayed only minimal Arc expression in the cortex (Fig. 2 *A*, *Bottom*; compare with seizure-free *APP/PS1Mertk*$^{-/-}$ mice in *SI Appendix*, Fig. S2*C*), and never developed seizures. Quantification revealed that ≥90% of NeuN^{+} neurons were Arc^{+} in the cortex, DG, CA3, and striatum of *APP/PS1Mertk*$^{-/-}$ mice after lethal seizure (Fig. 2*B*). This fraction was ≤10% in the striatum and DG of the same *APP/PS1Mertk*$^{-/-}$ mice in the absence of seizure, but consistent with the immunostaining in *SI Appendix*, Fig. S2*C*, was ∼35% in the cortex (Fig. 2*B*). The fraction of NeuN^{+} neurons that were Arc^{+} was ≤10% in all brain regions for *Mertk*$^{-/-}$ mice in the absence of seizure (Fig. 2*B*).

TAM Mutation Leads to the Accumulation of Apoptotic Cells in the DG. Together with the SVZ adjacent to the lateral ventricle, the DG of the hippocampus is a significant site of young adult neurogenesis in the mouse brain (27, 54). DG neurogenesis occurs during the first months of postnatal life, in a stem cell population that resides in its subgranular zone (SGZ). This SGZ is a thin layer of cells situated immediately beneath (interior to) the mature granular cell layer (GCL) (55), which is marked by very high cell density. (Dotted lines in Fig. 3*A* panels delimit the center of the GCL in the DG.) In the SGZ, it has been observed that ∼80% of newborn cells never survive to differentiate into DG granule cell neurons, but instead die by apoptosis within 10 d of their birth (56). These ACs are normally phagocytically cleared exclusively by microglia (56), and we have previously shown that microglia, both in the SGZ and the SVZ, require TAM receptors to effectively carry out AC clearance (28, 29). In the SGZ, for example, we have shown that *Axl*$^{-/-}$*Mertk*$^{-/-}$ mice display marked reductions in phagocytic index and capacity and a 2-fold increase in AC density and that tamoxifen-injected *Cx3cr1*$^{CreER/+}$*Mertk*$^{f/f}$ microglial-specific Mer knockouts (29) also display reductions in phagocytic index and capacity and a 1.6-fold increase in AC density (28). Similarly, we have previously shown that the dramatic accumulation of ACs seen in the *Axl*$^{-/-}$*Mertk*$^{-/-}$ SVZ is substantially phenocopied in the SVZ of tamoxifen-injected *Cx3cr1*$^{CreER/+}$*Mertk*$^{f/f}$ mice (29).

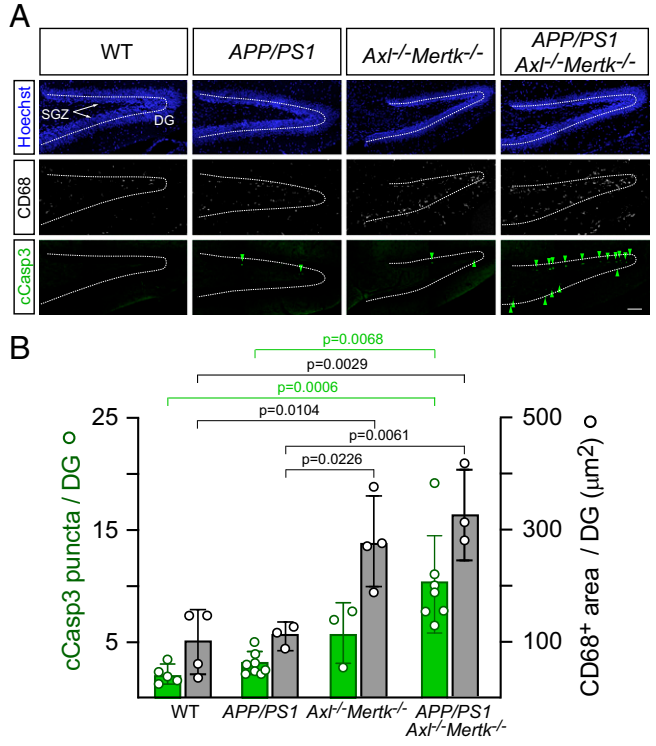

Fig. 3. Marked accumulation of apoptotic cells and activation of microglia in the P30 *APP/PS1Mertk*$^{-/-}$ dentate gyrus. (*A*) Representative sections through the DG of mice of the indicated genotypes stained for nuclei (Hoechst, blue, *Top*), the microglial activation marker CD68 (white, *Middle*), and the apoptotic cell marker cleaved Caspase-3 (cCasp3, green, *Lower*). The SGZ, where adult neurogenesis occurs, is arrowed, and the center of the GCL of the DG is marked by dotted lines. Note that most apoptotic cells in *APP/PS1 Axl*$^{-/-}$*Mertk*$^{-/-}$ mice accumulate in the SGZ (*Lower Right*). (*B*) Quantification of the results represented in *A*. Data in *B* and all subsequent figures in the paper are represented as mean ± 1 STD. Data are collected from five serial hippocampal sections per animal and n = 3 to 6 per genotype. One-way ANOVA test. (Scale bar, 100 µm.)

We used immunostaining for cleaved caspase 3 (cCasp3) to identify ACs, together with the lysosomal marker CD68 to monitor microglial activation, in the hippocampus of WT, *APP/PS1*, *Axl*$^{-/-}$*Mertk*$^{-/-}$, and *APP/PS1Axl*$^{-/-}$*Mertk*$^{-/-}$ mice (Fig. 3*A*). We performed this analysis at P30, near the onset of sudden death in all genotypes (Fig. 1). We found that while the density of cCasp3^{+} ACs in the DG exhibited a nonsignificant increase in *APP/PS1* mice relative to WT, the combination of *APP/PS1* with *Axl*$^{-/-}$*Mertk*$^{-/-}$ double mutation resulted in a remarkable 6-fold increase in the steady-state level of these dead cells (Fig. 3 *A* and *B*). This is in contrast to the 2-fold increase in AC density seen in *Axl*$^{-/-}$*Mertk*$^{-/-}$ alone. The area occupied by CD68^{+} microglial puncta was increased 3.3-fold in the *APP/PS1Axl*$^{-/-}$*Mertk*$^{-/-}$ DG relative to WT (Fig. 3 *A* and *B*). Essentially all CD68^{+} cells were Iba1^{+} microglia (*SI Appendix*, Fig. S3*A*), and consistent with our earlier work (29), the *Axl*$^{-/-}$*Mertk*$^{-/-}$ double mutation led to a marked increase in microglial Iba1 expression (*SI Appendix*, Fig. S3*B*). (This increase was especially prominent in the *APP/PS1Axl*$^{-/-}$*Mertk*$^{-/-}$ hippocampus; *SI Appendix*, Fig. S3*C*). Detailed examination revealed that nearly all of the AC accumulation in the *APP/PS1Axl*$^{-/-}$*Mertk*$^{-/-}$ DG occurred specifically in the SGZ (Fig. 3 *A*, *Lower Right*). As has been described previously (29), AC accumulation was exclusively seen in *Axl*$^{-/-}$*Mertk*$^{-/-}$ neurogenic regions and was undetectable elsewhere in the *Axl*$^{-/-}$*Mertk*$^{-/-}$ brain. Consistent with an extensive prior literature (57) and our own analyses in the SVZ (29), these ACs were NeuN^{-} but expressed the neural stem cell marker doublecortin (DCX) at both P30 and P90 (*SI Appendix*, Fig. S3*D*).

TAM Mutation Leads to Enhanced Survival of Newborn Neurons in the DG. Several lines of evidence indicate that phagocytosis by Mer-expressing microglia is not limited to their engulfment of ACs, but also extends to live cells that in response to a variety of stimuli externalize (express on their plasma membrane surface) the eat-me signal PtdSer (29, 58–61). This phagocytic engulfment of live cells has been termed "phagoptosis" (62). In the SVZ, the other major neurogenic center of the mouse brain, we have previously quantified the number of BrdU^{+} cells that appear in the wild-type versus *Axl*$^{-/-}$*Mertk*$^{-/-}$ olfactory bulb (OB), the site to which newborn SVZ cells migrate and differentiate, at 35 d after BrdU labeling (29). These BrdU^{+} cells in the OB were dividing in the SVZ at the time of labeling, had migrated along the rostral migratory stream, and then subsequently differentiated as neurons in the OB. We measured a 1.7-fold increase in BrdU^{+} cell density in the *Axl*$^{-/-}$*Mertk*$^{-/-}$ OB relative to wild-type 35 d after the labeling (29). None of these BrdU^{+} cells were apoptotic (cCasp3^{+}), nearly all of them were neurons as marked by expression of NeuN, and many expressed differentiation markers appropriate to their location in the OB (29).

We therefore performed similar BrdU pulse labelings in *APP/PS1* versus *APP/PS1Axl*$^{-/-}$*Mertk*$^{-/-}$ mice at either P30, when hippocampal neurogenesis is robust, or at P90, when neurogenesis is reduced (see below). We then quantified labeled cells at 28 and 7 d after the pulse. As illustrated in the representative example section shown in Fig. 4*A*, we counted BrdU$^+$ cells in both the SGZ and GCL and also in the entire DG (including the hilus and molecular layer). In the P90 series, we also stained sections for the proliferation marker Ki67 (Fig. 4*A*). As noted above, hippocampal neurogenic cell division occurs specifically in the SGZ, from which surviving cells subsequently migrate into the GCL and differentiate into neurons. At 28 d after a BrdU pulse applied at P30, we measured a ~2.1-fold increase in labeled cells in *APP/PS1Axl*$^{-/-}$*Mertk*$^{-/-}$ versus *APP/PS1* mice in both the SGZ + GCL and the full DG quantifications (Fig. 4 *B* and *C*). Note that, as expected, the large majority of BrdU$^+$ cells were located in the SGZ and GCL (Fig. 4 *B* and *C*). By 28 d after a BrdU pulse, most of the labeled cells that subsequently undergo apoptosis, together with live labeled cells that are engulfed by phagoptosis, have been cleared by microglial phagocytosis (28). These processes are not complete by 7 d after a pulse, and so we detected more labeled cells overall at 7 d after a BrdU pulse into P90 mice (Fig. 4 *D* and *E*). (Again at P90, essentially all BrdU$^+$ cells were present in the GCL and SGZ; *SI Appendix*, Fig. S3*E*). Correspondingly, we quantified an even greater disparity between *APP/PS1Axl*$^{-/-}$*Mertk*$^{-/-}$ and *APP/PS1* mice in these P90 experiments and measured ~3.5-fold more BrdU$^+$ or BrdU$^+$Ki67$^+$ cells in the former relative to the latter. Together, these results indicate that introducing TAM mutations into the *APP/PS1* line leads to the exuberant introduction of new cells into the GCL of the DG during the period of adult neurogenesis.

TAM Mutation Leads to Extra Mossy Fiber Synapses in CA3. All of the cells that survive and differentiate as a result of adult neurogenesis in the SGZ are excitatory glutamatergic neurons that project mossy fibers from the GCL to neurons in the hilus and the CA3 field of the hippocampus (63). We therefore asked whether the enhanced survival of newborn cells in the *APP/PS1Axl*$^{-/-}$*Mertk*$^{-/-}$ GCL resulted in more excitatory connections between the DG and CA3, leading to an excitatory/inhibitory imbalance. To address this question, we immunostained sections of the P30 *APP/PS1* and *APP/PS1Axl*$^{-/-}$*Mertk*$^{-/-}$ hippocampus with an antibody to the ZnT3 vesicular zinc transporter, which is expressed in the synaptic vesicles of GCL neurons and has previously been shown to intensely and specifically label presynaptic mossy fiber terminals in the hilus and CA3 (64, 65) (Fig. 5*A*). Hippocampal CA3 also receives excitatory glutamatergic input from entorhinal cortex and CA3 collaterals, but by using ZnT3 and focusing on CA3 proximal dendrites, we have almost exclusively assessed mossy fiber synapses. We simultaneously immunostained the same hippocampal sections with an antibody to PSD-95, which labels postsynaptic densities. We then used Airyscan superresolution imaging of the proximal region of CA3 pyramidal dendrites (box in Fig. 5*A*, enlarged in Fig. 5*B*), and Imaris software to construct ZnT3 and PSD-95 spheres (Fig. 5*C*) for synaptic quantification by proximity measurement of red (ZnT3) and

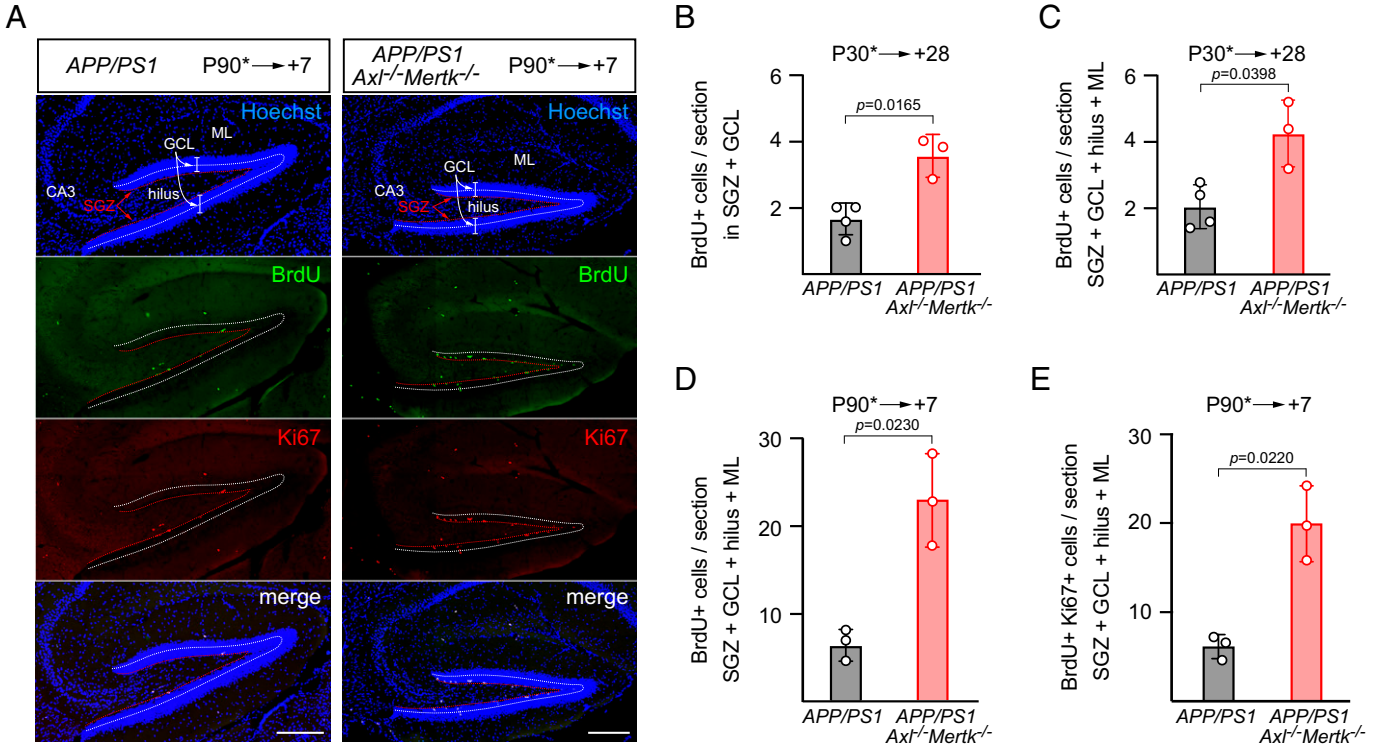

Fig. 4. Excess newborn cells in the *APP/PS1* and *APP/PS1Axl*$^{-/-}$*Mertk*$^{-/-}$ dentate gyrus. (*A*) Representative panels of the same sagittal sections through the V-shaped DG of *APP/PS1* (*Left* panels) and *APP/PS1Axl*$^{-/-}$*Mertk*$^{-/-}$ mice (*Right* panels) in which dividing cells were pulse labeled with BrdU at P90 and then analyzed 7 d later. *Top* row, cell nuclei labeled with the DNA dye Hoechst 33258; second row, BrdU-labeled nuclei visualized with an anti-BrdU antibody; third row, cells positive for the proliferation marker Ki67 visualized with an anti-Ki67 antibody; and *Bottom* row, merged images. Relevant hippocampal regions indicated in the *Top* panels are ML, molecular layer; GCL, granule cell layer; SGZ, subgranular zone; CA3, cornu ammonis field 3. Dotted lines indicate the center of the GCL (white) and the thin layer of the SGZ (red). (*B* and *C*) Quantification of BrdU$^+$ cells in the indicated regions of *APP/PS1* and *APP/PS1Axl*$^{-/-}$*Mertk*$^{-/-}$ mice pulse labeled at P30 and analyzed 28 d later. (*D* and *E*) Quantification of BrdU$^+$ cells in the indicated regions of *APP/PS1* and *APP/PS1Axl*$^{-/-}$*Mertk*$^{-/-}$ mice pulse labeled at P90 and analyzed 7 d later. Data are average from five serial hippocampal sections per animal and $n = 3$ to 4 per genotype. Unpaired *t* test. (Scale bars, 200 μm.)

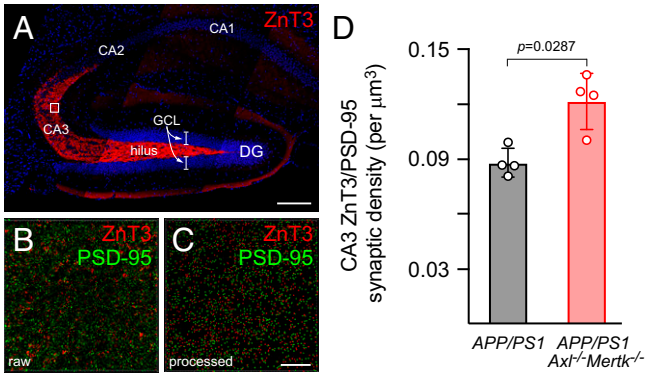

Fig. 5. Extra mossy fiber excitatory synapses in the *APP/PS1Mertk*$^{-/-}$ CA3. (*A*) Representative section of an *APP/PS1* hippocampus immunostained by ZnT3, which specifically labels DG mossy fiber terminals in the hilus and CA3. (*B*) Representative imaging field in hippocampal CA3 coimmunostained with ZnT3 (red) and PSD-95 (green); and (*C*) digital transformation of presynaptic puncta ZnT3 (red) and postsynaptic puncta PSD-95 (green). (*D*) Quantification of synaptic colocalization of ZnT3 and PSD-95 averaged from three or more images per section, four to five sections per animal (n = 4 for each genotype). Unpaired t test. (Scale bars, 200 µm in *A* and 10 µm in *B* and *C*.)

green (PSD-95) spheres (*Methods*). As is standard in the field, we defined synapses as ZnT3/PSD-95 sphere pairs that were ≤0.7 µm apart.

These analyses revealed that at 1 mo after birth, the CA3 proximal dendrite area of the *APP/PS1Axl*$^{-/-}$*Mertk*$^{-/-}$ hippocampus exhibits ∼38% more mossy fiber synapses than are seen in *APP/PS1* at the same age, as defined by ZnT3/PSD-95 coincidence (Fig. 5*D*). They are consistent with the neuronal differentiation of a subset of the excess BrdU^{+} cells seen in the *APP/PS1Axl*$^{-/-}$*Mertk*$^{-/-}$ hippocampus 28 d after a pulse labeling (Fig. 4), and with the subsequent development of neuronal connections between these GCL neurons and their synaptic targets in CA3.

Sudden Death Is Coincident with Neurogenesis but Anticorrelated with Plaques. The level of DG neurogenesis, which is largely restricted to young adulthood in both mice and humans, has previously been precisely measured over the first 9 mo of life in C57BL/6J mice (66). This is the strain onto which all of the mutations in Fig. 1 have been backcrossed and maintained. We therefore compared the time course of sudden death in *APP/PS1Gas6*$^{-/-}$ and *APP/PS1Mertk*$^{-/-}$ mice (Fig. 1) to the time course of expression of Ki67^{+} dividing cells and doublecortin-positive (DCX^{+}) cells in the C57BL/6J DG, as quantified previously (66). The number of both Ki67^{+} cells (*SI Appendix*, Fig. S4*A*) and DCX^{+} cells (*SI Appendix*, Fig. S4*B*) in the C57BL/6J DG exhibits an exponential decay from a high at 1 mo (P30) to much lower levels at 5 mo (P150) and beyond (*SI Appendix*, Fig. S4 *A* and *B*). We found that both of these exponential decays were highly correlated to the survival curves of *APP/PS1Gas6*$^{-/-}$ and *APP/PS1Mertk*$^{-/-}$ mice (*SI Appendix*, Fig. S4 *A* and *B*). That is, sudden death in these mice was highest when the rate of adult neurogenesis was highest, and fell, also approximately exponentially, as the rate of neurogenesis diminished (*SI Appendix*, Fig. S4 *A* and *B*).

At the same time that sudden death and hippocampal neurogenesis were coincident, we observed that sudden death and the development of dense-core amyloid plaques in all genotypes were strongly anticorrelated. We (and others) have previously quantified the development of dense-core Aβ plaques, as identified by staining with the amyloid dye ThioS, in *APP/PS1* mice over time (22). Our earlier analyses of cortical and hippocampal dense-core plaque burden began at 7 mo (22), after essentially all sudden death in *APP/PS1Axl*$^{-/-}$*Mertk*$^{-/-}$, *APP/PS1Mertk*$^{-/-}$, and *APP/PS1Gas6*$^{-/-}$ mice had already occurred (Fig. 1). We therefore extended our quantification of ThioS^{+} Aβ plaque burden to earlier time points and compared plaque development to sudden death over time. (We also included previously published sudden death data from *APP/PS1* mice lacking the interleukin-18 receptor, which similarly display enhanced early lethality relative to *APP/PS1* alone; ref 13). These analyses demonstrated that the cessation of early death in the *APP/PS1Axl*$^{-/-}$*Mertk*$^{-/-}$ mice coincided with the first detectable deposition of ThioS^{+} dense-core Aβ plaques (*SI Appendix*, Fig. S4*C*). No further sudden death was observed over the subsequent course of plaque accumulation in any line.

Discussion

Many investigators working with *APP/PS1* mice and other amyloidogenic mouse AD models have heretofore noted the occurrence of early sudden death in their colonies (12, 13, 17, 19, 22). The strong association between seizures and early AD notwithstanding, this early lethality has for the most part simply been ignored, since it occurs before the development of amyloid plaques and results in the loss of a relatively small number of experimental animals. At the same time, seizures early in the course of human AD are almost never fatal. The increase in early lethality upon the introduction of TAM system mutations into *APP/PS1* mice documented above is something that we of course observed during our previously published analyses of these mice (22), since it severely limited the number of animals that were available for study. We did not discuss this phenomenon at the time because our work was limited to a dissection of the role of TAM signaling in the microglia that surround Aβ plaques, and as shown above, the exacerbation of early *APP/PS1* lethality by TAM mutation occurs, just as in *APP/PS1* alone, before any plaques appear. In addition, we didn't have a mechanistic explanation for the phenomenon.

The results documented above indicate that this explanation involves an increased excitatory drive from the DG to CA3 target neurons in the hippocampus. We found that the DG was the single most heavily activated region of the brain in TAM-deficient *APP/PS1* mice after seizure. We further found that TAM system mutations allow for the survival and subsequent differentiation of an excess number of excitatory granule cell neurons in the DG—viable cells that would normally be cleared by TAM-dependent microglial phagocytosis (phagoptosis). This is essentially the same phenomenon and the same magnitude of effect that we have previously documented in the other center of adult neurogenesis in the mouse brain—the SVZ—where mutation of *Axl* and *Mertk* disables microglial phagocytosis and leads to the excess accumulation of viable newborn neurons in the olfactory bulb (29). The added cells that we detect in the DG may form additional synapses onto CA3 neurons, providing a hippocampal excitatory/inhibitory imbalance that feeds into the existing cortical hyperexcitability of *APP/PS1* mice. This ignites widespread firing across many regions of the TAM-deficient *APP/PS1* brain. It is noteworthy that after lethal seizure in *APP/PS1Mertk*$^{-/-}$ mice, the only hippocampal field other than the DG to display significant activation, as marked by elevated Arc expression, is CA3.

This hippocampal field is situated at a crucial location and plays an important role in the encoding of spatial representations and memory. Mossy fiber inputs from the DG pass highly integrated and sparsely coded cortical inputs on to CA3. As

such, this pathway and its synaptic connections are exceptionally susceptible to both seizures and the neurodegeneration that is exacerbated by Aβ-induced neuronal hyperactivity (67–69). AD patients with epileptic activity and seizures have been reported to have impaired cortical–hippocampal circuits and hastened cognitive decline (70–72); and in line with preclinical studies (18, 73), a recent phase IIa human clinical trial demonstrated that low-dose treatments with the anticonvulsive drug levetiracetam can improve deficits in hippocampal-mediated spatial memory and executive function specifically in AD patients who experience seizures and present with network hyperactivity (74).

Since we argue that the greatly enhanced lethality seen in *APP/PS1Axl*$^{-/-}$*Mertk*$^{-/-}$ mice relative to *APP/PS1* alone is due to compromised microglial phagocytosis, similar phenotypes might be predicted to develop in an amyloidogenic mouse AD model if phagocytic microglia were simply depleted from such a model before birth. An analysis of this form has very recently been reported (75). Kiani Shabastari et al. exploited a mouse line in which an essential enhancer element in the mouse colony stimulating factor 1 receptor (*Csf1r*) gene was deleted (76). Because microglia and many other tissue macrophages require continuous signaling through the CSF1 receptor for their survival (77, 78), deletion of this *Csf1r* enhancer element results in the embryonic ablation of microglia (76). When these *Csf1r* mutants lacking microglia (designated "FIRE mice") were crossed into the 5×FAD amyloidogenic AD model, it was observed that >50% of the compound mutants died from sudden death, and that most of this death occurred before P150 (75). The correspondence between this phenotype and the phenotype we describe above is striking. Like *APP/PS1* mice, 5×FAD mice exhibit a low incidence of sudden death before P150, and like *Axl*$^{-/-}$*Mertk*$^{-/-}$ mice (or *Mertk*$^{-/-}$ or *Gas6*$^{-/-}$ mice), FIRE mice display no lethality on their own (75). It is only when combined with the amyloidogenic *APP/PS1* and 5×FAD alleles that the sudden death contributions of the TAM system and FIRE mutations is revealed. Although Kiani Shabastari et al. did not provide a mechanistic explanation for the profound increase in early death seen when the FIRE enhancer mutation is introduced into the 5×FAD model (75), we propose that their death phenotype and ours are similar because both are tied to a deficit in microglial phagocytosis in the hippocampus.

Greatly enhanced early mortality, again due entirely to lethal seizures, has also been seen when the *APP/PS1* line is crossed with knockouts for the inflammatory cytokine interleukin-18 (IL-18) or its receptor (13). Cortical hyperexcitability and early lethal seizures in *APP/PS1IL18*$^{-/-}$ mice, which also can be effectively suppressed by levetiracetam, are associated with enhanced expression of excitatory synaptic proteins in the hippocampus, marked perturbations in hippocampal physiology, and increased sensitivity to the seizures that are chemically induced with picrotoxin (13). Anomalies in adult neurogenesis in the SGZ and DG similar to those that we have detected in *Axl*$^{-/-}$*Mertk*$^{-/-}$ mice, including an increased number of BrdU^{+} cells in the DG (relative to WT) at 24 h after a BrdU pulse, have also been reported for *IL18*$^{-/-}$ mice (79). With respect to these IL-18 effects, it is of interest to note that, within the brain, the only cells that express the full complement of NLRP3 components required to transduce IL-18 inflammatory signals are microglia. Since IL-18 receptors are predominantly expressed by neurons (80), a role for microglial IL-18 in the suppression of excitatory neurotransmission has also been advanced (13). Our results suggest that TAM-dependent microglial phagocytosis similarly suppresses the elaboration of exuberant excitatory connections between DG neurons and their targets in CA3.

Although mutations in the *Mertk* and *Gas6* genes dramatically increase the incidence of lethal seizures when crossed into *APP/PS1*, it is important to emphasize that these mutations only function as "second hits" (this is also the case for *IL-18* and *IL-18R* mutations when introduced into *APP/PS1* and for the FIRE mutation when introduced into 5×FAD) (13, 75). Seizure-induced sudden death is routinely observed in the *APP/PS1* line alone, but never in *Mertk*$^{-/-}$, *Axl*$^{-/-}$, *Gas6*$^{-/-}$, or *Axl*$^{-/-}$*Mertk*$^{-/-}$ mice. Thus, the key triggering event with respect to seizure induction in all cases is the production of excess Aβ from the mutant human transgenes present in the *APP/PS1* locus: The additional excitatory glutamatergic connections that we detect between the DG and CA3 are not on their own sufficient to trigger seizures. As previously described, excess Aβ is associated with sustained cortical and hippocampal hyperexcitability (12).

Why lethal seizures are not observed after ∼P150 in *APP/PS1* lines, with or without TAM mutations, remains a mystery. However, the observation that these seizures stop when dense-core plaques first appear is intriguing. It has previously been shown that the application of Aβ protofibrils to neurons in slice cultures of mouse cortex and hippocampus results in membrane depolarization (resting membrane potential elevation) and increased neuronal excitability (12). Recent work has shown that these protofibrils are normally phagocytosed by microglia, where they are routed to microglial lysosomes and then concentrated and aggregated (22, 77, 81, 82). This highly aggregated Aβ is finally deposited into the dense cores of dense-core plaques (81), and without microglia and microglial phagocytosis it now appears that these structures cannot be formed (77). As such, it seems possible that the cessation of seizures in *APP/PS1* mice may be due in part to the removal of seizure-inducing forms of Aβ polymers by microglial phagocytosis and their sequestration into dense-core plaques. The TAM RTKs are currently being therapeutically targeted—using antibody inhibitors, ligand traps, and small-molecule inhibitors of the TAM kinases—in the context of cancer, since the growth and metastasis of many different cancers are promoted by TAM up-regulation (83–85). The adverse effects that these potential therapeutics might have on microglial phagocytosis in the brain have not been considered.

Methods

Mice. The *Axl*$^{-/-}$ (23), *Mertk*$^{-/-}$ (23), *Axl*$^{-/-}$*Mertk*$^{-/-}$ (23), *Gas6*$^{-/-}$ (32), *Cx3cr1*^{CreER} (34), and *Mertk*$^{f/f}$ (29) mouse strains have been described previously. (Contact carla.rothlin@yale.edu for *Mertk*$^{f/f}$.) *B6.Cg-Tg(APPSwePSEN1dE9)* hemizygous mice (20, 21) (*APP/PS1*) (JAX No. 005864) were crossed with *Axl*$^{-/-}$, *Mertk*$^{-/-}$, *Axl*$^{-/-}$*Mertk*$^{-/-}$, *Gas6*$^{-/-}$, and/or *Cx3cr1*^{CreER}*Mertk*$^{fl/fl}$ lines. Recombination (inactivation) of the *Mertk*$^{f/f}$ allele in *Cx3cr1*$^{CreER/+}$*Mertk*$^{fl/fl}$ mice was achieved using tamoxifen injection at weaning at P28 to 30. *APP/PS1 Cx3cr1*$^{CreER/+}$ *Mertk*$^{fl/fl}$ mice received two doses (150 mg/kg body weight) of tamoxifen dissolved in 10% EtOH 90% filtered corn oil (Sigma) by intraperitoneal (IP) injection with the two successive injections 48 h apart. Control mice received two successive IP injections of vehicle (corn oil) alone. Mice were analyzed for Mer expression 1 wk, 2 mo, and 7 mo after the injection to ensure efficient and long-lasting Mer inactivation. All lines have been backcrossed for >10 generations to and maintained on a C57BL/6 background. All animal procedures were conducted according to protocols approved by the Salk Institute Animal Care and Use Committee (IACUC) (protocol No. 17-00009). Mice of both genders were randomly allocated to experimental groups unless otherwise noted.

Reagents and Antibodies. BrdU was from Sigma-Aldrich. Antibodies used were as follows: anti-mouse Axl (R&D AF854), anti-Mer (eBioscience DS5MMER and R&D AF591), anti-mouse Gas6 (R&D AF986), anti-BrdU (BU1/75 [ICR1], AbD serotec), anti-Iba1 (Wako 019-19741, 1:200, and Novus NB100-1028), anti-cleaved Casp3 (Asp175, Cell Signaling 9661), anti-doublecortin (DCX, Millipore ab2253), anti-ZnT3 (Sysy 197 002), anti-PSD-95 (Abcam ab18258), anti-CD68 (BioRad MCA1957), anti-NeuN (Chemicon MAB377), anti-Arc (Sysy #156003), anti-K_i-67 (Abcam ab15580), and anti-K_i-67 APC-conjugated (Invitrogen, clone SolA15). Secondary antibodies for immunohistochemistry were fluorophore-conjugated anti-rat (712- 545-153 and 712-165-153 from Jackson ImmunoResearch), anti-goat (A-11056 from Life Technologies, or 705-166-147 from Jackson Immuno Research), anti-guinea pig (Molecular Probe A-11073, and Jackson Immuno Research 706-165-148 and 706-175-148 were kind gifts from C.Kintner of the Salk Institute, La Jolla, CA, USA), anti-rabbit (A-10040 or A-21206 from Life Technologies and 711-606-152 from Jackson ImmunoResearch), and anti-mouse (A-21202 from Molecular Probe, 715-166-150 and 715-176-150 from Jackson ImmunoResearch). Key reagents and their usage were as follows: ThioS (Acros Organics 213150250), Hoechst 33258 in a 1% solution of bisbenzimide in water (Sigma-Aldrich B-2883), and paraformaldehyde (PFA) (Sigma P6148).

BrdU Pulse Labeling. Mice were administered a single dose of BrdU (100 mg/kg, dissolved in Dulbecco's phosphate-buffered saline (D-PBS)) intraperitoneally at P30 or P90 (28) and returned to their home cage. At 7 d or 28 d after BrdU injection, mice were anesthetized and their brains extracted using routine perfusion procedures as described previously (29).

Immunohistochemistry. Mice were anesthetized with a final concentration of 100 mg/kg ketamine/10 mg/kg xylazine in accordance with IACUC guidelines and were then transcardially perfused with 20 U/mL heparin in PBS followed by freshly prepared 4% PFA in PBS. Both brain hemispheres were postfixed in 4% PFA in PBS overnight and subsequently infiltrated in 30% sucrose in PBS for 1 d and flash frozen in Tris-buffer saline (TBS) tissue freezing medium (TFM) (General Data Healthcare TFM-5) using isopentane and kept at 80 °C until use. Frozen brain hemispheres were sagittally cryosectioned at 15 μm, air-dried overnight, and subsequently processed for staining. Antigen retrieval with citrate buffer was performed if needed by heating brain sections to 80 °C for 3 min in prewarmed citrate buffer and cooling to room temperature. Nonspecific binding was blocked by a 1-h incubation in blocking buffer (PBS containing 0.3% Triton X-100, 0.1% Tween-20, 5% donkey serum and 2% IgG-free bovine serum albumin (BSA)). Sections were incubated overnight at 4 °C with primary antibody diluted in blocking buffer, then washed in PBS 0.1% Tween-20 and incubated for 2 h at 22 to 24 °C in the dark with fluorophore-coupled secondary antibodies and subsequently in Hoechst for 5 min diluted in blocking buffer. Sections were washed, sealed with Fluoromount-G (SouthernBiotech), and stored at 4 °C. For immersion fixation methods, brains from mice found dead immediately after seizure or from control mice after receiving anesthesia until respiration ceased were freshly extracted after decapitation, split down the midline, and immediately immersion fixed in freshly prepared 4% PFA in PBS for 48 h. Brains were subsequently processed as for routinely perfused brains.

Dense-Core Plaque Labeling and Quantification. Cortical and hippocampal plaque density across the course of disease at the indicated timepoints was quantified by staining with the fluorescent amyloid dye thioflavin S (ThioS) as described previously (22). ThioS binds to the β-pleated sheets of dense-core amyloid plaques and provides for reliable semiautomated quantification of plaques. ThioS plaque density quantification was performed as described previously (22). Briefly, a serial set of 15-μm brain sagittal sections (six sections/mouse) was obtained 0.25 mm to 0.85 mm from the midline, each spaced 0.15 mm apart, and mounted directly on glass slides after cryosectioning. Serially cut sections from both hemispheres and various timepoints were used for measuring plaque density by histochemistry with ThioS staining using published protocols (86). Briefly, slides with brain sections were air-dried, then sequentially dehydrated in 70% and 80% ethanol before staining in filtered 1% ThioS dissolved in 80% ethanol in the dark. Slides were then rehydrated and washed sequentially in 80% ethanol, 70% ethanol, and water before being counterstained by Hoechst. ThioS-labeled brain sections were then either directly mounted or followed by further immunofluorescence staining, stored at 4 °C, and imaged within a week. Image analysis of the number of cortical and hippocampal ThioS$^+$ plaques was done blind with respect to genotypes and in a semiautomated fashion with set intensity thresholds for all conditions, using the "analyze particles" function in ImageJ or Fiji software.

Survival and Home-Cage Video Monitoring. Long-term (2 wk) continuous digital videos of young adult AD mice (1.5 to 3 mo) housed in their home cages with clear cage lids (two mice per cage) were collected at 25 fps using a high-resolution, infrared-equipped, digital video camera (Sony HandyCam HDR-XR520), set up in a top-down fixed angle for recording. The recording room was maintained on a 12-h/12-h light/red light cycle. Video monitoring of sporadic deaths and spontaneous convulsive seizures was performed by reviewing video footage via a VLC player. Cages were checked every 12 h to ensure proper air conduction, ample and accessible food and water, and to collect any mouse found dead. Brains from mice found dead during the study were freshly extracted, immersion fixed, and immunostained for Arc expression.

Confocal Microscopy. Fluorescent immunostaining images were acquired with a Zeiss LSM 710 confocal microscope using Plan-Apochromat 20× 0.8-NA air-matched or 63× 1.4-NA oil objectives (laser lines: 405 nm, 488 nm, 594 nm, and 633 nm). Image size was 1,024 × 1,024 pixels. For quantification of Arc$^+$NeuN$^+$ cells in various brain regions, two representative single-plane images, at 320 μm × 320 μm per section from two sections per biological sample, were randomly taken from striatum, DG, CA3, or layers 3 to 4 of prefrontal cortex using Hoechst as an unbiased channel. For synaptic analysis, Airyscan superresolution images were acquired with a Zeiss LSM 880 Rear Port Laser Scanning Confocal and Airyscan FAST Microscope using 63× oil-immersion objective and piezo z-stage for superresolution imaging. Three images from five serial brain sections per animal containing CA3 apical dendrites were imaged as 8-bit images at 2,124 pixels × 2,124 pixels and 53.98 μm × 53.98 μm as a z stack of seven slices with a total thickness of 1.29 μm. Exposure acquisition was set according to the nonmutant samples and all sections were imaged within the same session. Images were obtained and processed via the Zen Black edition. Images for cortical and hippocampal plaque quantification were acquired with an Olympus VS-120 Virtual Slide Scanning Microscope.

Data Analysis. For fixed-brain thin sections, maximum intensity projection images of 212 μm × 212 μm (1,024 × 1,024 pixel resolution) were analyzed in Fiji. Approximately five to seven plaques per brain sections (three to five sections per animal) were randomly chosen in the prefrontal cortex using the 6E10 channel. For analyses in the P30 DG, tiled and stitched maximum intensity projection images from field of view of 640 μm × 1,280 μm (1,024 × 1,024 pixel resolution) that fully captured the DG were used for cCasp3 number and area analysis using particle analysis in Fiji with a 3 μm^2 minimum cutoff. Higher magnification images 212 μm × 212 μm (1,024 × 1,024 pixel resolution), which centers on dentate gyrus/SGZ were used for CD68 area analysis in P30 DG. For adult neurogenesis analysis in hippocampus using BrdU, the analysis of neurogenesis in vivo was performed as described previously (28, 87) Five sagittal sections from one series per animal of each genotype containing the same area of hippocampus were analyzed in all experiments. Proliferating cells were assessed by BrdU$^+$ and K_i-67$^+$ cell quantification and neuroblasts were assessed by DCX$^+$ cell quantification, while mature neurons were assessed by NeuN$^+$ cell quantification. The proliferation of either of these populations was quantified by their colocalization with BrdU or K_i-67 using the software ImageJ (Fiji). Analysis of synapse number was performed blind to genotype using IMARIS software (version 9.1.2, bitplane). Synapses were defined as proximity of the postsynaptic PSD-95 puncta to presynaptic ZnT3 puncta. The z stacks of each condition (*APP/PS1* or *APP/PS1 Axl*$^{-/-}$ *Mertk*$^{-/-}$) were presented as three-dimensional volumes acquired by Airyscan superresolution imaging. Puncta from each channel were defined in each channel as spheres of average diameter of 0.5 μm using the spot detection function. The colocalization of spots from different channels within a distance from center to center of spots of 0.7 μm was quantified as a synapse. Synapse number from each image was averaged across five sections per animal.

Statistical Analysis. Statistics were performed with GraphPad Prism (version 8.0) software.

Data, Materials, and Software Availability. All study data are included in the article and/or supporting information.

ACKNOWLEDGMENTS. We thank P. G. Burrola and J. Hash for technical assistance, John Karlstad of the Salk Animal Resources Department and Sarah Parylak for technical support with respect to home-cage monitoring studies, and Axel Nimmerjahn and members of the G.L. laboratory and the Molecular Neurobiology Laboratory for discussions. This work was supported by grants from the NIH (RF1 AG060748), the Cure Alzheimer's Fund, the Coins for Alzheimer's Research Trust, and Ferring Pharmaceuticals (to G.L.); and by Salk Women in Science Award and Goeddel Chancellor's, Marguerite Vogt, and H.A. and Mary K. Chapman Charitable Trust graduate fellowships (to Y.H.).

1. W. A. Hauser, M. L. Morris, L. L. Heston, V. E. Anderson, Seizures and myoclonus in patients with Alzheimer's disease. *Neurology* **36**, 1226–1230 (1986).
2. D. C. Hesdorffer, W. A. Hauser, J. F. Annegers, E. Kokmen, W. A. Rocca, Dementia and adult-onset unprovoked seizures. *Neurology* **46**, 727–730 (1996).
3. M. F. Mendez, P. Catanzaro, R. C. Doss, R. ARguello, W. H. Frey, 2nd, Seizures in Alzheimer's disease: Clinicopathologic study. *J. Geriatr. Psychiatry Neurol.* **7**, 230–233 (1994).
4. J. C. Amatniek *et al.*, Incidence and predictors of seizures in patients with Alzheimer's disease. *Epilepsia* **47**, 867–872 (2006).
5. D. A. Lozsadi, A. J. Larner, Prevalence and causes of seizures at the time of diagnosis of probable Alzheimer's disease. *Dement. Geriatr. Cogn. Disord.* **22**, 121–124 (2006).
6. A. D. Lam *et al.*, Association of epileptiform abnormalities and seizures in Alzheimer disease. *Neurology* **95**, e2259–e2270 (2020).
7. M. Romoli, A. Sen, L. Parnetti, P. Calabresi, C. Costa, Amyloid-β: A potential link between epilepsy and cognitive decline. *Nat. Rev. Neurol.* **17**, 469–485 (2021).
8. F. Cortini, C. Cantoni, C. Villa, Epileptic seizures in autosomal dominant forms of Alzheimer's disease. *Seizure* **61**, 4–7 (2018).
9. K. A. Vossel *et al.*, Seizures and epileptiform activity in the early stages of Alzheimer disease. *JAMA Neurol.* **70**, 1158–1166 (2013).
10. M. A. Busche, A. Konnerth, Impairments of neural circuit function in Alzheimer's disease. *Philos. Trans. R. Soc. Lond. B Biol. Sci.* **371**, 20150429 (2016).
11. A. Nakamura *et al.*, Early functional network alterations in asymptomatic elders at risk for Alzheimer's disease. *Sci. Rep.* **7**, 6517 (2017).
12. R. Minkeviciene *et al.*, Amyloid beta-induced neuronal hyperexcitability triggers progressive epilepsy. *J. Neurosci.* **29**, 3453–3462 (2009).
13. T. C. Tzeng *et al.*, Inflammasome-derived cytokine IL18 suppresses amyloid-induced seizures in Alzheimer-prone mice. *Proc. Natl. Acad. Sci. U.S.A.* **115**, 9002–9007 (2018).
14. S. Mondragón-Rodríguez *et al.*, Phosphorylation of Tau protein correlates with changes in hippocampal theta oscillations and reduces hippocampal excitability in Alzheimer's model. *J. Biol. Chem.* **293**, 8462–8472 (2018).
15. S. F. Kazim *et al.*, Early-onset network hyperexcitability in presymptomatic Alzheimer's disease transgenic mice is suppressed by passive immunization with anti-human APP/Aβ antibody and by mGluR5 blockade. *Front. Aging Neurosci.* **9**, 71 (2017).
16. A. Cheng *et al.*, SIRT3 haploinsufficiency aggravates loss of GABAergic interneurons and neuronal network hyperexcitability in an Alzheimer's disease model. *J. Neurosci.* **40**, 694–709 (2020).
17. K. K. Hsiao *et al.*, Age-related CNS disorder and early death in transgenic FVB/N mice overexpressing Alzheimer amyloid precursor proteins. *Neuron* **15**, 1203–1218 (1995).
18. P. E. Sanchez *et al.*, Levetiracetam suppresses neuronal network dysfunction and reverses synaptic and cognitive deficits in an Alzheimer's disease model. *Proc. Natl. Acad. Sci. U.S.A.* **109**, E2895–E2903 (2012).
19. J. J. Palop *et al.*, Aberrant excitatory neuronal activity and compensatory remodeling of inhibitory hippocampal circuits in mouse models of Alzheimer's disease. *Neuron* **55**, 697–711 (2007).
20. J. L. Jankowsky *et al.*, Co-expression of multiple transgenes in mouse CNS: A comparison of strategies. *Biomol. Eng.* **17**, 157–165 (2001).
21. J. L. Jankowsky *et al.*, Mutant presenilins specifically elevate the levels of the 42 residue beta-amyloid peptide in vivo: Evidence for augmentation of a 42-specific gamma secretase. *Hum. Mol. Genet.* **13**, 159–170 (2004).
22. Y. Huang *et al.*, Microglia use TAM receptors to detect and engulf amyloid β plaques. *Nat. Immunol.* **22**, 586–594 (2021).
23. Q. Lu *et al.*, Tyro-3 family receptors are essential regulators of mammalian spermatogenesis. *Nature* **398**, 723–728 (1999).
24. Q. Lu, G. Lemke, Homeostatic regulation of the immune system by receptor tyrosine kinases of the Tyro 3 family. *Science* **293**, 306–311 (2001).
25. G. Lemke, Biology of the TAM receptors. *Cold Spring Harb. Perspect. Biol.* **5**, a009076 (2013).
26. K. Obernier, A. Alvarez-Buylla, Neural stem cells: Origin, heterogeneity and regulation in the adult mammalian brain. *Development* **146**, dev156059 (2019).
27. J. T. Gonçalves, S. T. Schafer, F. H. Gage, Adult neurogenesis in the hippocampus: From stem cells to behavior. *Cell* **167**, 897–914 (2016).
28. I. Diaz-Aparicio *et al.*, Microglia actively remodel adult hippocampal neurogenesis through the phagocytosis secretome. *J. Neurosci.* **40**, 1453–1482 (2020).
29. L. Fourgeaud *et al.*, TAM receptors regulate multiple features of microglial physiology. *Nature* **532**, 240–244 (2016).
30. J. J. Neher *et al.*, Phagocytosis executes delayed neuronal death after focal brain ischemia. *Proc. Natl. Acad. Sci. U.S.A.* **110**, E4098–E4107 (2013).
31. E. D. Lew *et al.*, Differential TAM receptor-ligand-phospholipid interactions delimit differential TAM bioactivities. *eLife* **3**, e03385 (2014).
32. A. Angelillo-Scherrer *et al.*, Deficiency or inhibition of Gas6 causes platelet dysfunction and protects mice against thrombosis. *Nat. Med.* **7**, 215–221 (2001).
33. J. J. Miner *et al.*, The TAM receptor Mertk protects against neuroinvasive viral infection by maintaining blood-brain barrier integrity. *Nat. Med.* **21**, 1464–1472 (2015).
34. C. N. Parkhurst *et al.*, Microglia promote learning-dependent synapse formation through brain-derived neurotrophic factor. *Cell* **155**, 1596–1609 (2013).
35. A. Zagórska *et al.*, Differential regulation of hepatic physiology and injury by the TAM receptors Axl and Mer. *Life Sci. Alliance* **3**, e202000694 (2020).
36. H. Keren-Shaul *et al.*, A unique microglia type associated with restricting development of Alzheimer's disease. *Cell* **169**, 1276–1290.e17 (2017).
37. A. D. Umpierre, L. J. Wu, How microglia sense and regulate neuronal activity. *Glia* **69**, 1637–1653 (2021).
38. M. E. Tremblay *et al.*, The role of microglia in the healthy brain. *J. Neurosci.* **31**, 16064–16069 (2011).
39. T. G. Beach, W. B. Woodhurst, D. B. MacDonald, M. W. Jones, Reactive microglia in hippocampal sclerosis associated with human temporal lobe epilepsy. *Neurosci. Lett.* **191**, 27–30 (1995).
40. M. G. Drage, G. L. Holmes, T. N. Seyfried, Hippocampal neurons and glia in epileptic EL mice. *J. Neurocytol.* **31**, 681–692 (2002).
41. L. A. Shapiro, L. Wang, C. E. Ribak, Rapid astrocyte and microglial activation following pilocarpine-induced seizures in rats. *Epilepsia* **49** (suppl. 2), 33–41 (2008).
42. Z. Yin *et al.*, Immune hyperreactivity of Aβ plaque-associated microglia in Alzheimer's disease. *Neurobiol. Aging* **55**, 115–122 (2017).
43. E. R. Roy *et al.*, Type I interferon response drives neuroinflammation and synapse loss in Alzheimer disease. *J. Clin. Invest.* **130**, 1912–1930 (2020).
44. M. Garcia-Alloza *et al.*, Characterization of amyloid deposition in the APPswe/PS1dE9 mouse model of Alzheimer disease. *Neurobiol. Dis.* **24**, 516–524 (2006).
45. I. Shemer *et al.*, Non-fibrillar beta-amyloid abates spike-timing-dependent synaptic potentiation at excitatory synapses in layer 2/3 of the neocortex by targeting postsynaptic AMPA receptors. *Eur. J. Neurosci.* **23**, 2035–2047 (2006).
46. G. Powell, B. Ziso, A. J. Larner, The overlap between epilepsy and Alzheimer's disease and the consequences for treatment. *Expert Rev. Neurother.* **19**, 653–661 (2019).
47. K. A. Vossel, M. C. Tartaglia, H. B. Nygaard, A. Z. Zeman, B. L. Miller, Epileptic activity in Alzheimer's disease: Causes and clinical relevance. *Lancet Neurol.* **16**, 311–322 (2017).
48. H. E. Scharfman, The dentate gyrus and temporal lobe epilepsy: An "Exciting" era. *Epilepsy Curr.* **19**, 249–255 (2019).
49. A. D. Madar *et al.*, Deficits in behavioral and neuronal pattern separation in temporal lobe epilepsy. *J. Neurosci.* **41**, 9669–9686 (2021).
50. C. G. Dengler, D. A. Coulter, Normal and epilepsy-associated pathologic function of the dentate gyrus. *Prog. Brain Res.* **226**, 155–178 (2016).
51. N. Plath *et al.*, Arc/Arg3.1 is essential for the consolidation of synaptic plasticity and memories. *Neuron* **52**, 437–444 (2006).
52. M. K. Chawla *et al.*, Sparse, environmentally selective expression of Arc RNA in the upper blade of the rodent fascia dentata by brief spatial experience. *Hippocampus* **15**, 579–586 (2005).
53. M. W. Jung, B. L. McNaughton, Spatial selectivity of unit activity in the hippocampal granular layer. *Hippocampus* **3**, 165–182 (1993).
54. T. Toda, F. H. Gage, Review: Adult neurogenesis contributes to hippocampal plasticity. *Cell Tissue Res.* **373**, 693–709 (2018).
55. L. C. Abbott, F. Nigussie, Adult neurogenesis in the mammalian dentate gyrus. *Anat. Histol. Embryol.* **49**, 3–16 (2020).
56. A. Sierra *et al.*, Microglia shape adult hippocampal neurogenesis through apoptosis-coupled phagocytosis. *Cell Stem Cell* **7**, 483–495 (2010).
57. G. Kempermann, H. Song, F. H. Gage, Neurogenesis in the adult hippocampus. *Cold Spring Harb. Perspect. Biol.* **7**, a018812 (2015).
58. G. Lemke, How macrophages deal with death. *Nat. Rev. Immunol.* **19**, 539–549 (2019).
59. K. Segawa *et al.*, Phospholipid flippases enable precursor B cells to flee engulfment by macrophages. *Proc. Natl. Acad. Sci. U.S.A.* **115**, 12212–12217 (2018).
60. Y. Tufail *et al.*, Phosphatidylserine exposure controls viral innate immune responses by microglia. *Neuron* **93**, 574–586.e8 (2017).
61. J. Brelstaff, A. M. Tolkovsky, B. Ghetti, M. Goedert, M. G. Spillantini, Living neurons with Tau filaments aberrantly expose phosphatidylserine and are phagocytosed by microglia. *Cell Rep.* **24**, 1939–1948.e1934 (2018).
62. G. C. Brown, J. J. Neher, Microglial phagocytosis of live neurons. *Nat. Rev. Neurosci.* **15**, 209–216 (2014).
63. N. Toni, A. F. Schinder, Maturation and functional integration of new granule cells into the adult hippocampus. *Cold Spring Harb. Perspect. Biol.* **8**, a018903 (2015).
64. J. J. McAuliffe *et al.*, Altered patterning of dentate granule cell mossy fiber inputs onto CA3 pyramidal cells in limbic epilepsy. *Hippocampus* **21**, 93–107 (2011).
65. R. D. Palmiter, T. B. Cole, C. J. Quaife, S. D. Findley, ZnT-3, a putative transporter of zinc into synaptic vesicles. *Proc. Natl. Acad. Sci. U.S.A.* **93**, 14934–14939 (1996).
66. N. M. Ben Abdallah, L. Slomianka, A. L. Vyssotski, H. P. Lipp, Early age-related changes in adult hippocampal neurogenesis in C57 mice. *Neurobiol. Aging* **31**, 151–161 (2010).
67. L. M. Yu, D. Polygalov, M. E. Wintzer, M. C. Chiang, T. J. McHugh, CA3 synaptic silencing attenuates kainic acid-induced seizures and hippocampal network oscillations. *eNeuro* **3**, ENEURO.0003-16.2016 (2016).
68. M. A. Yassa *et al.*, High-resolution structural and functional MRI of hippocampal CA3 and dentate gyrus in patients with amnestic Mild Cognitive Impairment. *Neuroimage* **51**, 1242–1252 (2010).
69. L. Mucke, D. J. Selkoe, Neurotoxicity of amyloid β-protein: Synaptic and network dysfunction. *Cold Spring Harb. Perspect. Med.* **2**, a006338 (2012).
70. A. D. Lam *et al.*, Silent hippocampal seizures and spikes identified by foramen ovale electrodes in Alzheimer's disease. *Nat. Med.* **23**, 678–680 (2017).
71. K. A. Vossel *et al.*, Incidence and impact of subclinical epileptiform activity in Alzheimer's disease. *Ann. Neurol.* **80**, 858–870 (2016).
72. J. Noebels, A perfect storm: Converging paths of epilepsy and Alzheimer's dementia intersect in the hippocampal formation. *Epilepsia* **52** (suppl. 1), 39–46 (2011).
73. J. Q. Shi *et al.*, Antiepileptics topiramate and levetiracetam alleviate behavioral deficits and reduce neuropathology in APPswe/PS1dE9 transgenic mice. *CNS Neurosci. Ther.* **19**, 871–881 (2013).
74. K. Vossel *et al.*, Effect of levetiracetam on cognition in patients with Alzheimer disease with and without epileptiform activity: A randomized clinical trial. *JAMA Neurol.* **78**, 1345–1354 (2021).
75. S. Kiani Shabestari *et al.*, Absence of microglia promotes diverse pathologies and early lethality in Alzheimer's disease mice. *Cell Rep.* **39**, 110961 (2022).
76. R. Rojo *et al.*, Deletion of a Csf1r enhancer selectively impacts CSF1R expression and development of tissue macrophage populations. *Nat. Commun.* **10**, 3215 (2019).
77. E. Spangenberg *et al.*, Sustained microglial depletion with CSF1R inhibitor impairs parenchymal plaque development in an Alzheimer's disease model. *Nat. Commun.* **10**, 3758 (2019).

78. M. R. Elmore *et al.*, Colony-stimulating factor 1 receptor signaling is necessary for microglia viability, unmasking a microglia progenitor cell in the adult brain. *Neuron* **82**, 380–397 (2014).
79. K. Yamanishi *et al.*, Interleukin-18-deficient mice develop hippocampal abnormalities related to possible depressive-like behaviors. *Neuroscience* **408**, 147–160 (2019).
80. S. Alboni, D. Cervia, S. Sugama, B. Conti, Interleukin 18 in the CNS. *J. Neuroinflammation* **7**, 9 (2010).
81. S. H. Baik, S. Kang, S. M. Son, I. Mook-Jung, Microglia contributes to plaque growth by cell death due to uptake of amyloid β in the brain of Alzheimer's disease mouse model. *Glia* **64**, 2274–2290 (2016).
82. C. Condello, P. Yuan, A. Schain, J. Grutzendler, Microglia constitute a barrier that prevents neurotoxic protofibrillar Aβ42 hotspots around plaques. *Nat. Commun.* **6**, 6176 (2015).
83. R. M. Linger, A. K. Keating, H. S. Earp, D. K. Graham, TAM receptor tyrosine kinases: Biologic functions, signaling, and potential therapeutic targeting in human cancer. *Adv. Cancer Res.* **100**, 35–83 (2008).
84. P. Msaouel, G. Genovese, J. Gao, S. Sen, N. M. Tannir, TAM kinase inhibition and immune checkpoint blockade- a winning combination in cancer treatment? *Expert Opin. Ther. Targets* **25**, 141–151 (2020).
85. M. Vouri, S. Hafizi, TAM receptor tyrosine kinases in cancer drug resistance. *Cancer Res.* **77**, 2775–2778 (2017).
86. P. T. Ly, F. Cai, W. Song, Detection of neuritic plaques in Alzheimer's disease mouse model. *J. Vis. Exp.* **53**, 2831 (2011).
87. J. M. Encinas, G. Enikolopov, Identifying and quantitating neural stem and progenitor cells in the adult brain. *Methods Cell Biol.* **85**, 243–272 (2008).